

Supplementary information

Universality in consolidation of colloidal gels

Saikat Roy and Mahesh S Tirumkudulu

Department of Chemical Engineering,

Indian Institute of Technology Bombay, Powai, Mumbai, 400076, India

This note gives details of the simulation methodology and results, and model derivation.

SIMULATION PROCEDURE

Simulations of uniaxial compression of flocculated colloidal particulate networks were performed using open source codes, Large-scale Atomic/Molecular Massively Parallel Simulator (LAMMPS, [1]) and LIGGGHTS (LAMMPS Improved for General Granular and Granular Heat Transfer Simulations, [2]). Temporal and spatial evolution of the colloidal gel under compression will be effected by both hydrodynamic and elastic forces. Since the focus is on determining the elastic modulus in uniaxial compression, the yield stress, and the yield strain of the network, very small strain rates were used. The ratio of the drag force on a particle during compression to the elastic force in the network, $\eta\dot{\epsilon}/G\epsilon$, gives a measure of the strength of hydrodynamic forces over elastic forces. Here, η is the solvent viscosity, G is the particle modulus, ϵ is the strain while $\dot{\epsilon}$ is the strain rate. For, $\eta = 10^{-3}$ Pa s, $G = 10^5 - 10^{11}$ Pa, $\epsilon = 0.01$, and $\dot{\epsilon} = 10^{-5}$ s⁻¹, the aforementioned dimensionless quantity is negligible. An experimental study of aggregating colloidal gels [3] has shown that under very small sedimentation velocities, fluid flow through the gel network does not lead to rearrangement of the particle structure suggesting that the dynamics is determined by the contact mechanics. Interestingly, the shear rates in their case were very low and similar to those in our simulation, $\dot{\epsilon} \sim 10^{-5}$ s⁻¹. In view of such experiments and the analysis of relative forces discussed earlier, our simulations exclude hydrodynamic forces.

Monodisperse dispersion of spherical particles of diameter, D , are placed randomly in a three dimensional box of dimension, $30D$ (along x), $30D$ (along y) and $200D$ (along z). The periodic boundary condition is applied in x and y directions. The upper and lower walls of the box are made of a single layer of identical particles having the same properties as those of the network while periodic boundary condition is applied on the sides. Initially, all particles are placed randomly and

Brownian motion is incorporated to achieve a flocculated particle network. Uniaxial compression is achieved by bringing the top and bottom enclosing walls together at a constant speed, V_0 . Gilabert *et al.* [4] suggest that to eliminate dynamical effects, the strain rates should be small, with the condition that the product of the inertial timescale, $\sqrt{mD/F_0}$, and the maximum strain rate should be less than 0.05. Here, m is the mass of the particles and F_0 is attraction force between particles. In our case, the maximum strain rate of $2 \times 10^{-5} \text{ s}^{-1}$ is more than three orders lower than that obtained from the aforementioned condition. We have also simulated the same system with a higher strain rate (10^{-4} s^{-1}) and found no change in the properties of interest. So inertial effects are eliminated in the slow compression limit. The volume fraction (ϕ) at any time is calculated by dividing the total particle volume by the volume of the box at that instant of time.

Since the simulations used open source codes whose details are readily available [1, 2], only a brief description of the simulation procedure will be provided here. The contact model is similar to that used in the classic work of Cundall and Strack [5] where friction force is taken into account for the sliding mode. In addition, the influence of rolling resistance (RR) is also implemented. We assume that the interactions between the particles is short range so that a central constant attraction force, F_0 , acts only when the gap between the particles goes to zero. Thus, F_0 is the measure of the maximum tensile force a contact will support before breaking off. Both electrostatic interactions and contact plasticity are ignored. The particle deformation is assumed to be Hookean where the normal repulsive elastic force, $F_N^{e,ij} = -k_n \delta n_{ij}$, acts when the particles overlap, that is, when $\delta n_{ij} < 0$. Here, δn_{ij} is the overlap distance of two interacting particles labelled i and j , and k_n is the normal stiffness coefficient. We define a dimensionless parameter, $F_0/k_n D$, to characterize the elastic deformation under attraction.

Additionally, viscous damping is implemented in the normal direction to achieve equilibrium configuration at each strain. The viscous damping force (along with a repulsive Hookean force) acts when two particles approach each other and start to overlap. The viscous retardation along with the strong attractive force eventually bonds the particles together. We ensured that the inertia of the moving particles does not influence the consolidation process by performing simulations at varying strain rates (all small) and confirmed that the results were identical. As in the case of the normal force, the elastic part of the tangential force at contact, F_T^{ij} , is a linear function of the elastic part of the total relative tangential displacement, with the proportionality constant being the tangential stiffness coefficient, k_t . Sliding takes place when F_T^{ij} is greater or equal to $\pm \mu F_N^{e,ij}$ where μ is the coefficient of friction. Note that the Coulomb inequality applies to the repulsive elastic

TABLE I: Simulation parameters rendered dimensionless by the particle diameter, D , the normal stiffness, k_n , and the speed of the walls, V_0 .

$\frac{F_0}{k_n D}$	$\frac{k_t}{k_n}$	μ	μ_r	$\frac{V}{V_0}$
0.005, 0.025	1	0.5	0.5	0.6

part of the normal force only.

Experiments performed by Furst and Pantina [6] and Pantina and Furst [7] on bending mechanics of flocculated colloidal aggregates show that single-bonded aggregates are able to support torques, confirming the existence of substantial rolling resistance between the adjacent colloidal particles. The elasticity of linear colloidal particle aggregates was measured using a three-point bending geometry, where the two end particles were held in stationary laser traps, and a bending moment was applied by translating a trap positioned on the center particle at a fixed velocity perpendicular to the aggregate. If particles did undergo free rotations, one would expect the aggregates to respond to the bending moment by forming a triangle like structure with a pivot point at the center particle. Instead, the observed shape was similar to that expected from a thin rigid rod under similar load conditions suggesting that single particle bonds are capable of supporting torques.

The origin of the rolling friction is attributed to deformation of the surfaces under contact and the fore-aft asymmetry (about the vertical diameter) in the contact area when one particle tries to move past the other[9]. Consequently for a rotating sphere on a plane surface (see Fig. 1), the reaction force F_r acts at a point slightly ahead of the vertical diameter. Since the normal force (F_n) acts along the vertical diameter, a restoring torque opposing the rotation of magnitude, $F_r d$

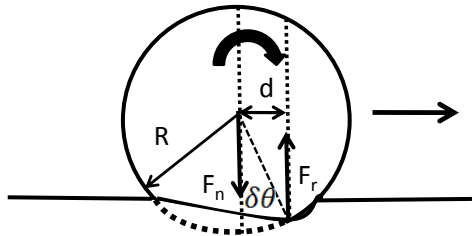


FIG. 1: Schematic of the Rolling Resistance: F_n is the normal force, F_r is the reaction force and d is the distance between the line of action of two force. The dotted curve represents the undeformed section of the sphere in the absence of contact. The sphere rotates in the anti-clockwise direction and has a tendency to move to the right.[8]

is generated, where d is the distance between the line of force of F_r and F_n . Note that F_r and F_n form a force couple. For the case considered here, one may imagine d to increase from zero under static condition to a finite value when an external torque is exerted by the neighboring particle. In such a case, the rolling resistance will increase linearly with d till a maximum value of $F_n d_{max}$ is reached, after which the particle will roll. The distance between the pair of forces can be related to the angle $\delta\theta$, $d = R\delta\theta$. The angle $\delta\theta$ is related to the rolling torque via a torsional spring constant.

In the simulations, the torque exerted by particle i on its neighbor j , M_{ij} , can be divided into two parts, one due to the tangential contact force and the other due to the resistance to rolling, M_{ij}^r ,

$$M_{ij} = -\frac{F_T^{ij}D}{2} + M_{ij}^r. \quad (1)$$

The rolling resistance is modeled similar to the contact elasticity and friction for the sliding mode where the rolling torque is related to the angular displacement of a torsional spring,

$$M_{ij}^r = k_r \delta\theta_r. \quad (2)$$

Here, k_r is the the rolling stiffness of the torsional spring and $\delta\theta_r$ denotes the incremental relative rotation between the particles. The *epsd2* model of LIGGGHTS is implemented where the rolling stiffness, k_r , is related to the tangential stiffness coefficient,

$$k_r = \frac{k_t D^2}{4}. \quad (3)$$

The rolling torque is limited by the full mobilization torque, $M_{ij}^{r,m}$,

$$M_{ij}^{r,m} = \frac{\mu_r D F_N^{e,ij}}{2}, \quad (4)$$

where μ_r is the rolling friction, so that the rolling occurs when $M_{ij} \geq M_{ij}^{r,m}$. No viscous damping is implemented for the rolling mode. The simulation parameters are summarized in Table I. The above conditions for sliding and rolling are similar to that of Gilabert *et al.* [4] and unlike those of Seto *et al.* [10] who apply threshold forces and torques to break contacts between particles. Given that the order of magnitude of the dispersion force for a $1 \mu\text{m}$ particle is $F_0 \sim 10^{-8}$ N (Table I), the ratio of the dispersion force to the elastic force is $O(10^{-3})$ which similar to the order of $F_0/(k_n D)$

considered in the simulation. Note that this also implies that the extent of particle deformation due to the attraction alone is small compared to the particle size.

We start the simulation with a dilute dispersion ($\phi = 0.06$) and start compressing the system slowly. Brownian motion causes the particles to flocculate and the flocs are brought closer by the moving walls. Once the flocs connect to form a percolating particle network, Brownian motion has little effect on the consolidation process since the attractive potential is much higher than the Brownian forces, $F_0 r / k_B T \gg 1$, where $r \sim 1-2$ nm is the typical distance between the surfaces of contacting particles. We have considered a values of $V/V_0 = 0.6$, where V is the characteristic velocity due to Brownian motion, and is given by, $V = \sqrt{k_B T / m}$ (Table I). Recall that the speed of the moving walls, V_0 , is kept fixed. It is important to note that in all simulations, the compression was started well below the gelation concentration.

The simulations were performed with 20000 particles and with many different initial configurations but we observed very small variation (less than 5%) in properties of interest. Therefore, the results were obtained from three separate simulations for a fixed condition.

Compression of the strongly aggregated colloidal gel network is carried out at a slow rate. In order to obtain the compressive yield stress, the yield strain, and the elastic modulus (in uniaxial compression) at a fixed volume fraction, the wall velocity is set to zero and the walls are allowed to move freely enabling the particle networks to relax. This ensures that the stress, as measured at the walls, is negligible before the compression process is restarted. Next, the network is compressed with a small incremental strain ($O(10^{-3})$) and held fixed. All the wall force components in the z -direction are summed up which on division by the wall area gives the compressive stress at that volume fraction. It is ensured the stress value thus obtained does not vary with time before applying the next incremental strain. The elastic modulus of the packing is determined from the stress versus strain profile obtained from the slow, stepwise compression so that the network undergoes purely elastic deformation. We ensure that static equilibrium has been reached at each confining strain so that the stress measured at the top and bottom walls are equal (within a difference of 0.01%). The same simulation also provides the yield strain wherein the network is decompressed by moving the walls outward in a stepwise manner to ensure that all the strain is recovered. The critical value beyond which the entire strain is not recovered is the yield strain and the corresponding stress is the yield stress. The network is next compressed beyond the yield strain to a new volume fraction and the process of compression and decompression is repeated at the new volume fraction to determine the elastic modulus, the yield strain and the yield stress. The

gelation concentration is inferred from the existence of a finite elastic modulus of the network. The consolidation process is studied at volume fractions beyond the gelation volume fraction, $\phi > 0.08$ since there are large uncertainties in the yield stress values at volume fractions close to gelation, as has also been reported earlier [10].

The simulation studies of Gilabert *et al.* [4] and Seto *et al.* [10] have used the fractal model [11, 12] to evaluate the packing characteristics of the gel network. It is shown that the entire system space is filled with flocs of a certain fractal dimension with a correlation length which corresponds to the size of the floc. Here, in addition to studying the fractal structure as done previously, we also investigate how the average contact number changes with the volume fraction.

RESULTS AND DISCUSSION

Particle arrangement

Figure 2 presents the contact distribution at four different concentrations, $\phi=0.145, 0.23, 0.29$ and 0.34 in the presence of RR. Interestingly, there is very little change in the distribution for all but the highest concentrations. Consequently, the average coordination number increases incrementally from 3.76 to 4.11 when the corresponding volume fraction increases from 0.145 to 0.34.

We also plot contact distribution for a fixed volume fraction and for two different values of attraction (Fig. 3).

In Fig. 4, we plot the average coordination number versus volume fraction obtained from simulations.

Before closing this section, we determine the fractal properties of the packing. In this case, the interest is to determine the characteristic particle chain length that form the fractal network. We determine the correlation length at each volume fraction above which the particle network looks uniform. Following Masschaele *et al.* [13] and Seto *et al.* [10], the particle density was determined in cubical boxes of increasing lengths so that the density becomes invariant of the box size when the size exceeds the correlation length, the latter corresponding to the characteristic chain length. Because of the finite size of the computational domain, the correlation length for a fixed volume fraction corresponds to the box size where the ratio of the standard deviation of the local density and the global density is 0.5. The correlation length (q) is plotted as a function of the volume

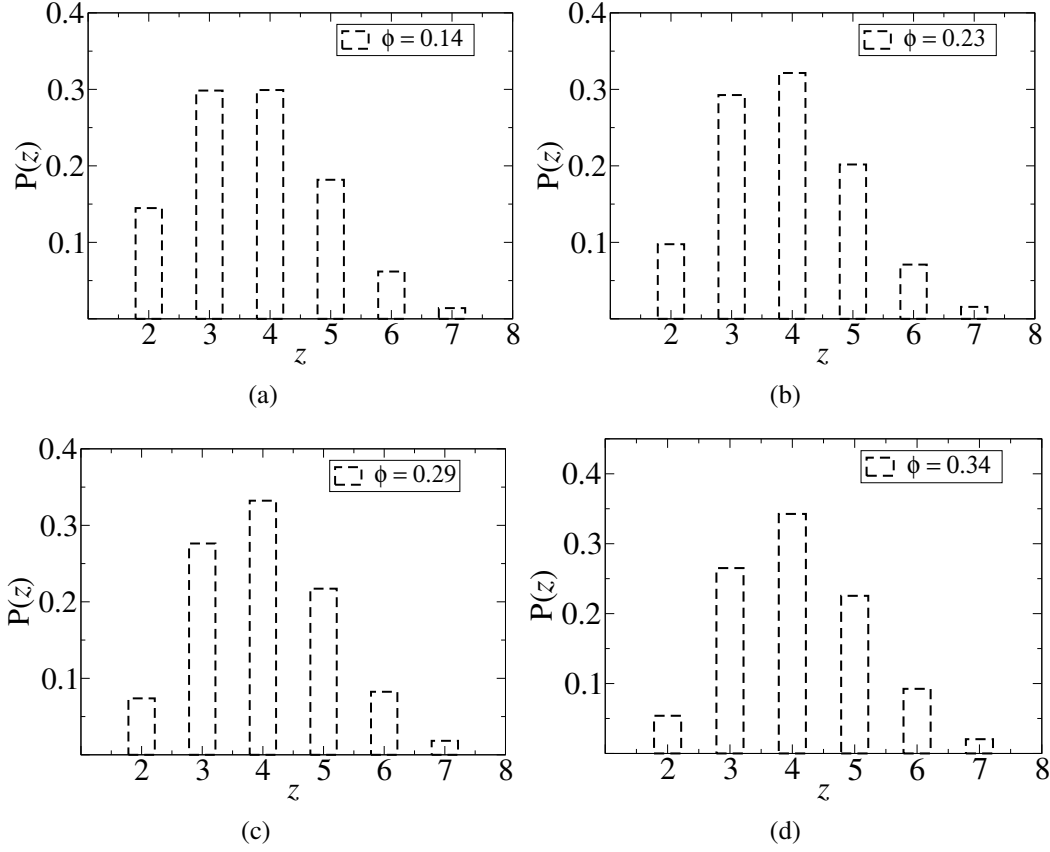


FIG. 2: Contact distribution comparison in presence of RR, (a) $\phi = 0.145$, (b) $\phi = 0.23$, (c) $\phi = 0.29$, (d) $\phi = 0.34$; Here $\frac{F_0}{k_n D} = 0.005$.

fraction in Fig 5. The q versus ϕ follows a power-law relation with an exponent of approximately, -1.55. If a fractal network was assumed, then the data can be fit to a power-law relation where the exponent is given by $-1/(d - d_f)$, with d_f being the fractal dimension and d , the Euclid dimension. The fractal dimensions are found to be 2.3.

Mechanical Properties of Particle Packing

The elastic modulus of the network was determined by decompressing the system at each volume fraction and then compressing it slowly in a step wise manner to generate the stress versus strain profile at that volume fraction. The initial profile is linear and the slope gives the elastic modulus of the network under compression. Figure 6 presents the dimensionless normal stress ($\sigma D/k_n$) in the vertical direction measured at the top/bottom plate versus strain at very low and high volume fractions. As the strain is increased at a fixed volume fraction, the network undergoes

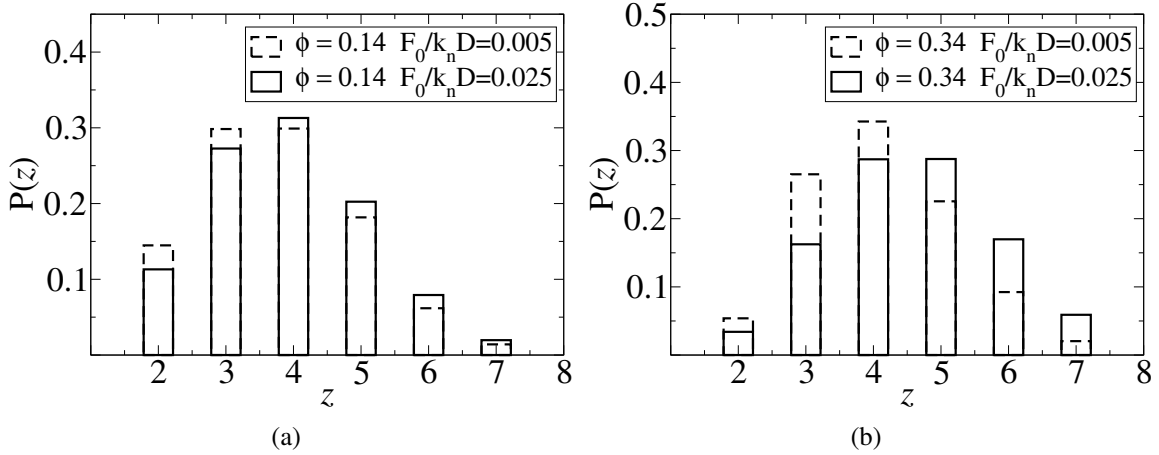


FIG. 3: Contact distribution comparison for two different volume fractions for varying attractions, (a) $\phi = 0.145$, (b) $\phi = 0.34$. Simulation parameters are the same as for Fig. 2.

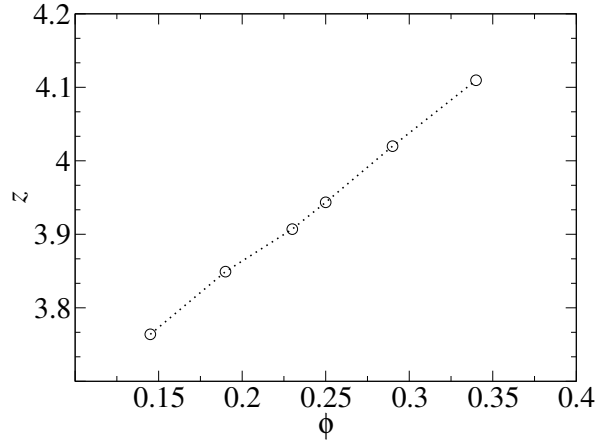


FIG. 4: z vs ϕ profile obtained from simulation

plastic deformation beyond a critical strain and is represented by the non-linear section of the profile. When the system is decompressed from this stage, not all the strain is recovered. If we set the yield strain by the 0.1% offset method [14], the yield strain values are about 0.0183 and 0.023 at $\phi = 0.145$ and 0.34, respectively. On the other hand, the yield stress increases by two orders of magnitude over the same range of volume fractions suggesting that the increase in yield stress is essentially determined by the elastic modulus of the particle network.

The yield strains for the entire range of volume fraction are plotted in Fig. 7(a). The yield strain changes by only about 15% about its average value(0.02) over the entire range. Interestingly, these results are in accordance with the experiments of Buscall *et al.* [15] who measured the compressive yield stress for flocculated dispersions of latex and attapulgite clay. Their observed variation

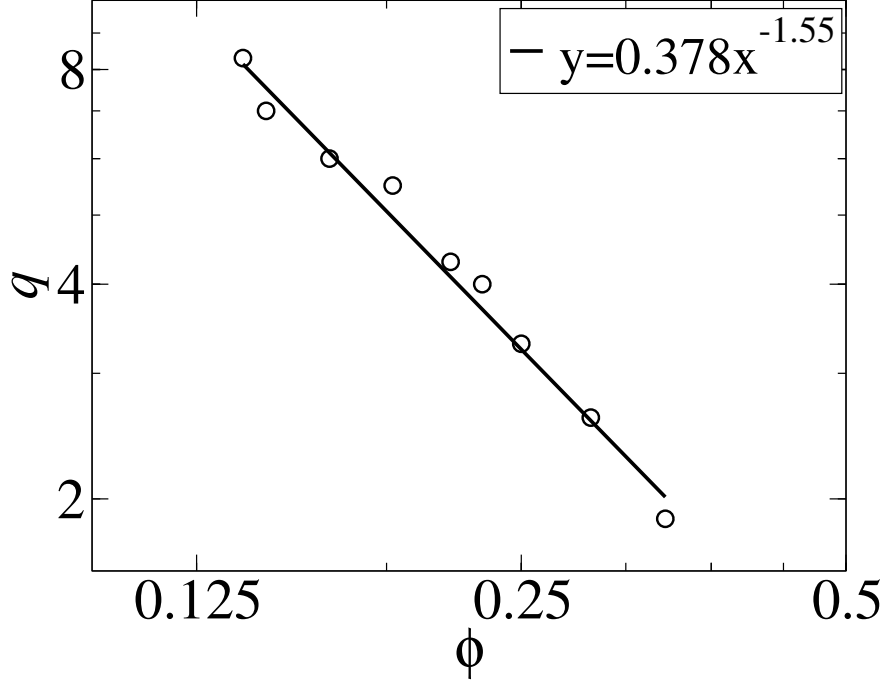


FIG. 5: The correlation length, q is plotted as a function of ϕ with Power law fit. Simulation parameters are the same as that mentioned in Fig. 2

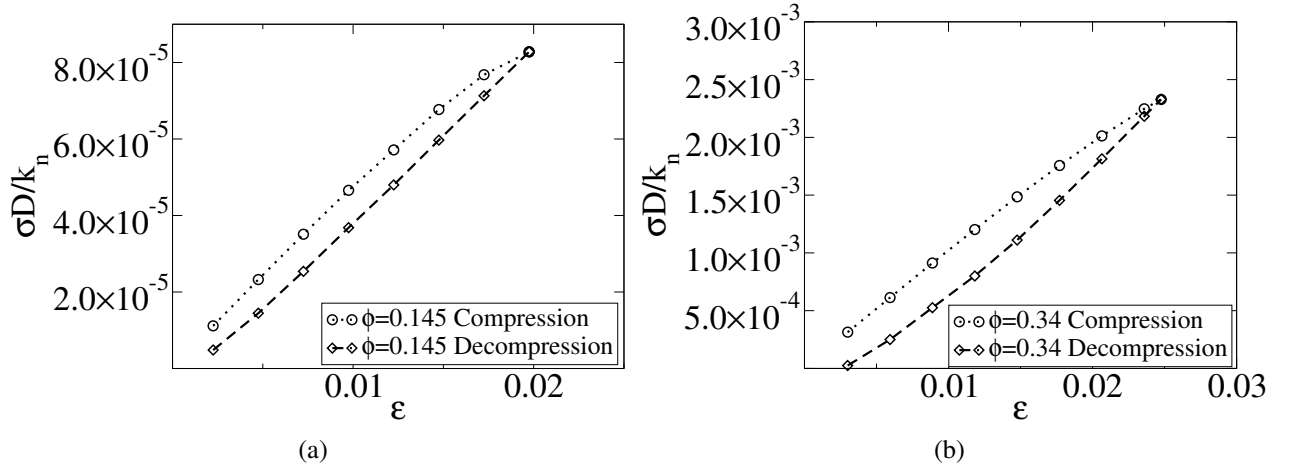


FIG. 6: Stress vs strain curve at (a) $\phi = 0.145$ (b) $\phi = 0.34$

of the compressive yield stress and the shear modulus of the network with volume fraction suggests that the elastic limit of the networks in terms of strain is independent of volume fraction for volume fractions beyond gelation. In other words, the experiments imply that the yield strain is independent of volume fraction.

The slope of the linear region in the stress versus strain profile gives the elastic modulus of the packing (G) under uniaxial compression. Figure 7(b) plot the elastic modulus, for two different

values of the attraction force. Clearly, the modulus values are very similar at both attraction force magnitudes, implying that the elastic modulus does not scale with attraction at least for the range studied.

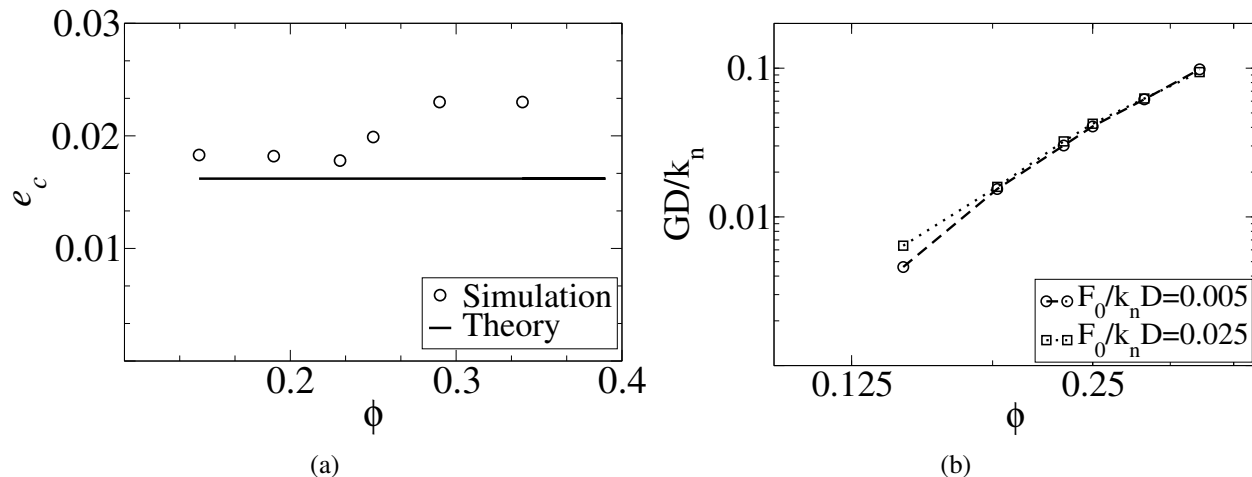


FIG. 7: (a) Yield strain vs volume fraction (b) Elastic modulus as a function of volume fraction for two different attraction.

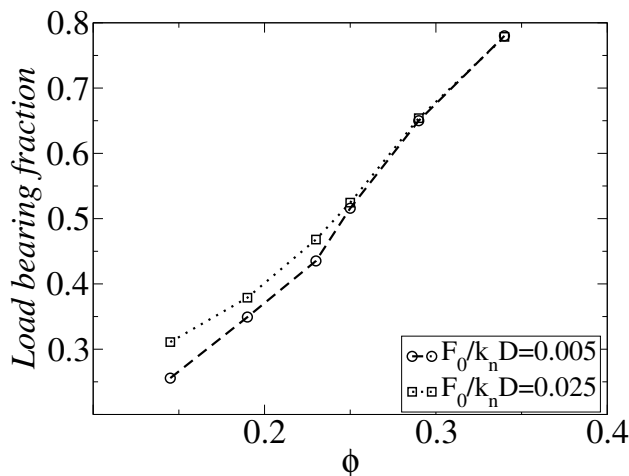


FIG. 8: Fraction of load bearing particles versus packing fraction for low and high attraction.

At this stage, it is informative to determine the fraction of particles that bear most of the load during compression. In the elastic regime when an incremental load is applied to the network, not all particles contribute equally to the increase in elastic energy of the network. Simulations of Radjai *et al.* [16] on the deformation of two dimensional granular particles (cohesion-less) have shown that during compaction, there are two types of particle networks - strong networks which carry the whole deviatoric load and weak networks which essentially behave as an interstitial

liquid. This suggests that it is the former that will contribute to the elastic modulus. To determine the particles/contacts that contribute most to the deformation and therefore to the elastic modulus, we determined the contacts that contribute 95% of the total elastic energy rise upon an incremental strain. Here, both the tangential and normal forces were accounted for in the calculations. The 95% criteria is used to plot the fraction of load bearing particles for a range of volume fractions and for two different attraction forces (Fig. 8). Interestingly, the percentage of the load bearing particles at a given volume fraction changes very slightly with attraction for both cases.

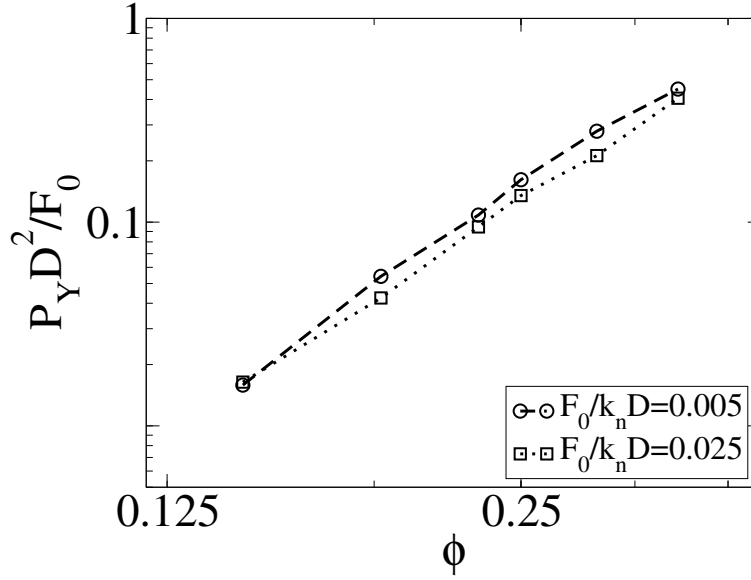


FIG. 9: Dimensionless compressive yield stress versus volume fraction as a function of attraction

Fig. 9 plots the non-dimensional compressive yield stress for two different attractive forces. The average slope of 3.95 obtained from the above plot is similar to the experimental results of Buscall *et al.* [15] who observed a slope of 4 ± 0.5 over a volume fraction range of 0.05 to 0.3 for flocculated dispersions.

THEORY

Consider space filling aggregate of spheres, each of diameter D , with an average particle density of N/V in a volume, V . Let n_j to be the unit vector from the center of an arbitrary sphere to a contact point on its circumference. The rectangular cartesian components of the unit vector n_j are $(\cos(\varphi) \sin(\theta), \sin(\varphi) \sin(\theta), \cos(\theta))$, where θ is the polar angle from the axis of symmetry.

To determine the critical strain, we assume that the deformation is affine, i.e. the strain at the

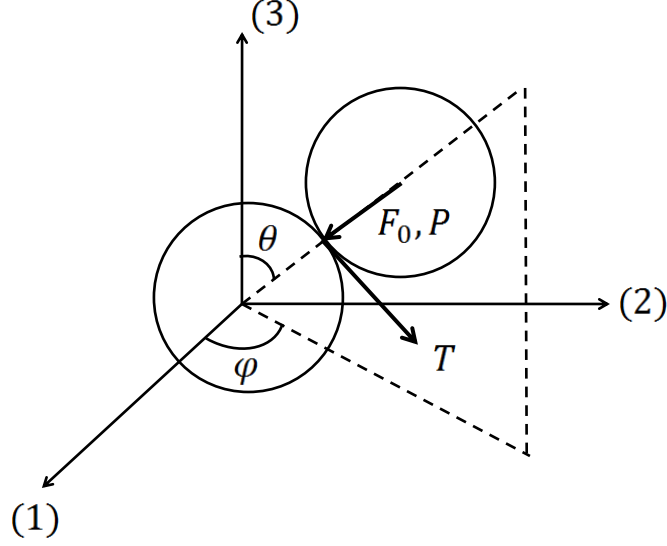


FIG. 10: Schematic of a pair of particles. Here, P and F_0 are, respectively, the radial contact force due to the external stress and interparticle attraction, while T is the contact force in the tangential direction

particle pair level is the same as that of macroscopic length scale. The displacement u_i of a contact point relative to the center of the sphere is given in terms of e_{ij} , macroscopic strain applied at the boundary. The displacement is related linearly to the strain,

$$u_i = \frac{D}{2} e_{ij} n_j \quad (5)$$

In this work, we shall consider the uniaxial compressive strain in the ‘3’ direction so that the strain tensor becomes,

$$e_{ij} = -\delta_{3i} \delta_{j3} e_o$$

where the negative sign accounts for the compression and $e_o > 0$ is the uniaxial strain. The displacement of the contact point is then obtained as,

$$u_i = \frac{D}{2} e_{ij} n_j = \left(-e_o \cos^2(\theta) \hat{e}_r + e_o \sin(\theta) \cos(\theta) \hat{e}_\theta \right) \frac{D}{2} \quad (6)$$

where the magnitude of the normal component of the displacement, δ , of the contact point is

$$\delta = \frac{D}{2} e_o \cos^2(\theta), \quad (7)$$

while the tangential component is

$$s = \frac{D}{2} e_o \sin(\theta) \cos(\theta). \quad (8)$$

The total contact force $F_i(\mathbf{n})$ exerted by a neighboring sphere at a contact point consists of two parts, namely, normal components due to an externally imposed strain, P , and a tangential component, T_i , due to the external strain,

$$F_i = -Pn_i + T_i. \quad (9)$$

Further, since T_i is perpendicular to n_i , we have

$$T_i n_i = 0. \quad (10)$$

Since the displacement at the particle level is due to the externally imposed strain, the force components that originate from the external strain is related to the components of the displacement. For small displacements, the magnitude of the normal component of contact force is assumed to vary linearly with the normal displacement of the contact point,

$$P = k_n \delta \quad (11)$$

where k_n is the normal stiffness coefficient. Similarly the magnitude of the tangential component of the force is related to the tangential displacement,

$$T = k_t s \quad (12)$$

when T is less than the critical value required for the sphere to slide, $T_r = \mu(P + F_0)$; the latter being the expression for Coulomb friction. The inter-particle attractive force is represented by F_0 with the assumption that this force exists only when the particles are in contact. Here, k_t is the tangential stiffness coefficient and μ is the friction coefficient for sliding.

Now, at the onset of sliding, the critical tangential displacement of the contact point is given

by,

$$\begin{aligned} s^E &= \frac{T_r}{k_t} = \frac{\mu(P + F_0)}{k_t} = \frac{\mu(k_n\delta + F_0)}{k_t} \\ &= \bar{\mu}\delta + \frac{\mu F_0}{k_t} \end{aligned} \quad (13)$$

where $\bar{\mu} \equiv \mu k_n/k_t$. Thus the critical angle for the onset of sliding (θ_r) can be obtained by substituting the expressions for δ and s from (7) and (8) into (13),

$$\frac{D}{2}e_o \sin(\theta_r) \cos(\theta_r) = \bar{\mu} \frac{D}{2}e_o \cos^2(\theta_r) + \frac{\mu F_0}{k_t}$$

The above equation can be rearranged so as to yield a quadratic equation in $\tan(\theta)$,

$$\frac{2\mu F_0}{k_t D e_o} \tan^2(\theta_r) - \tan(\theta_r) + \bar{\mu} + \frac{2\mu F_0}{k_t D e_o} = 0 \quad (14)$$

For fixed values of parameters ($D, \bar{\mu}, F_0, k_t$), the above equation will yield real solutions only above a critical value of the applied strain. In other words, no slip is possible for strains below the critical value so that the entire deformation is elastic in nature. The expression for the critical strain is obtained by enforcing the condition that the roots of equation (14) be real,

$$e_c = \frac{4\mu F_0}{k_t D (-\bar{\mu} + \sqrt{\bar{\mu}^2 + 1})} \quad (15)$$

The above analysis considers the existence of only sliding friction. However, past experiments have shown that when ends of a particle chain are held fixed and the central particle is subject to a bending moment, the chain bends like a thin rigid rod under similar conditions. The absence of rolling between neighboring particles points to the pinning of the solid-solid contact line and therefore the existence of a rolling resistance. If we assume in our analysis that there exists rolling resistance at the point of contact in addition to sliding, the torque exerted at the contact point, given by the product of the tangential force and the particle radius, should be greater than a critical value for the particle to roll. Consequently, at the critical torque,

$$\theta^E = \frac{T_r D}{2k_r} = \frac{\mu_r (k_n\delta + F_0) D}{2k_r} \quad (16)$$

where μ_r is the rolling friction coefficient, k_r is the rolling stiffness, and θ^E is the critical angle

beyond which the neighboring particle rolls permanently. Since the contacts are expected to be stiffer in the presence of rolling resistance, we assume a simple model where the sliding stiffness spring and the rolling stiffness spring are in parallel. Consequently, the sliding displacement is equal to the rolling displacement which in turn is equal to the tangential displacement obtained from the affine strain,

$$s = \frac{D}{2}\delta\theta = \frac{D}{2}e_o \sin(\theta) \cos(\theta).$$

where $\delta\theta$ is the angular displacement of the contact point around the particle, and is related to the tangential strain causing the rotation, $T_r = k_r(D/2)\delta\theta$. In the numerical simulations presented in part 1, the rotational stiffness is related to the tangential stiffness as,

$$k_r = k_t D^2/4$$

which implies that the tangential force causing the tangential and rotation displacements are equal and the sum of the two gives the total tangential force. Further, if the rolling friction coefficient (μ_r) is taken to be the same as the sliding friction coefficient (μ), rolling and sliding occur at the same critical tangential stress and so the critical strain for yielding both with and without rolling resistance will be the same. However, for different values of μ_r and μ , the network will yield depending on which of the two critical conditions is met first. For sake of simplicity, we shall take $\mu = \mu_r$, so that equation (14) applies to both sliding and rolling.

Now, in order to account for the nonaffineness in the deformation field we build on the formulation of Kantor and Webman [17] who determined the macroscopic elastic moduli of an elastic percolating network close to percolation. The deformation of the links between the particles are characterized by a bending stiffness coefficient (G) and a normal stiffness coefficient (Q). By considering an arbitrary force acting at one end of a chain (with the other fixed), they determined the displacements of each particle of the chain that would minimize the total energy of the system. In this way, strain at the level of the links were allowed to be different from that at the ends. The effective normal stiffness of the chain was obtained as, $k_n = Q/DL_{\parallel}$, where L_{\parallel} is proportional to the square of the sum of component of all links (i.e. between consecutive contacts) along the direction of external force while the effective tangential stiffness of the chain was, $k_t = G/N_c S_{\perp}^2$, where N_c is the number of particles in the chain, and S_{\perp} is the radius of gyration of the projection of the links in direction perpendicular to the external force. For very long chains, i.e. when N_c is very large, all energy is stored in tangential displacement of the chain with very little deformation in

stretching/compression of particles along the force direction.

Since the criteria of minimization of the elastic energy allows non-affine motion of individual particles forming the chain and constrains only the ends of the chains to follow the affine deformation, we apply the aforementioned model to the current case of strongly aggregating dispersion. As reported in the simulations, the characteristic correlation length for the particle concentration exhibits a power-law relation with the volume fraction. If the network structure is assumed to be monofractal with the characteristic chain length being the correlation length, which is a function of the particle volume fraction, then we have, $q/D \sim \phi^{-1/(d-d_f)}$, where d is the Euclid dimension, and d_f is the fractal dimension. Further, the number of particles in the chain are related to the correlation length, $N_c \sim (q/D)^{d_1}$, where d_1 ranges from 1 for straight chains to 1.6 for chains formed via self-avoiding random walk [18]. Assuming $DL_{\parallel} \sim D^2 N_c$ and $S_{\perp} \sim q$ (see, for example, Nakayama *et al.* [19]), the scaling of the effective tangential and normal stiffness of the chain is obtained as,

$$k_t \sim \phi^{\frac{2+d_1}{d-d_f}}, \quad k_n \sim \phi^{\frac{d_1}{d-d_f}},$$

For a constant fractal dimension for a network of chains, the effective tangential stiffness would be smaller than the effective normal stiffness. Note that, Potanin and Russel [18] applied the model of Kantor and Webman [17] to describe the rheology of weakly aggregating colloidal dispersions but considered only the tangential stiffness of the network.

In order to derive the constitutive relation, we consider the network to be made of particle chains of length q and obtain the stress tensor by averaging over a representative volume of order q^3 ,

$$\sigma_{ij} = -2qn_c z_c \alpha \int_0^{2\pi} \int_0^{\pi/2} E(\theta, \varphi) F_i n_j \sin(\theta) d\theta d\varphi$$

where the number density of the chains, n_c , is related to the number of particles in the chain and the volume fraction, $n_c N_c = \phi/(\pi D^3/6)$, while z_c is the coordination number of the chains. Since particle contacts are isotropic, the same is expected of the chains that means $E(\theta, \varphi) = 1/4\pi$. The deformation is assumed to be affine at the length scale of the chains, that is the displacement at the macroscopic scale is the same at the level of the chains. Now, the normal stress in the ‘3’ direction is given by,

$$\sigma_{33} = -qn_c z_c \alpha \int_0^{\pi/2} (-Pn_3 + T_3)n_3 \sin(\theta) d\theta \quad (17)$$

where the first term in the integral simplifies to,

$$\int_0^{\pi/2} (Pn_3n_3)\sin(\theta)d\theta = \frac{k_{n,c}qe_o}{5} \quad (18)$$

while the second term becomes

$$\int_0^{\pi/2} T_3n_3\sin(\theta)d\theta = m \int_0^{\theta_r} k_{t,c}s_3n_3\sin(\theta)d\theta - \int_{\theta_r}^{\pi/2} \mu P \sin(\theta)n_3 \sin(\theta)d\theta, \quad (19)$$

where $m = 1$ is for the case when only sliding is present while $m = 2$ accounts for both rolling and sliding. Note that for the tangential part, the integration is divided into two regions, namely, $(0 < \theta < \theta_r)$ and $(\theta_r < \theta < \frac{\pi}{2})$ since the tangential force follows a different relationship before the start of slipping/rolling and after slipping/rolling starts. The rectangular components of tangential displacement are,

$$s_3 = -qe_o \sin^2(\theta) \cos(\theta).$$

On substituting the above expressions in (19) gives the following individual terms,

$$\begin{aligned} \int_0^{\theta_r} k_{t,c}s_3n_3 \sin(\theta)d\theta &= -k_{t,c}qe_o \left[\frac{2}{15} - (\cos^3(\theta_r) - \cos^5(\theta_r)) \right] \\ \int_{\theta_r}^{\pi/2} \mu P \sin(\theta)n_3 \sin(\theta)d\theta &= \mu k_{n,c}qe_o [\cos^3(\theta_r) - \cos^5(\theta_r)] \end{aligned} \quad (20)$$

One of the main quantities of interest is the compressive yield stress which is the applied normal stress beyond which the packing deforms plastically. In our calculations, the compressive yield stress is equal to the the stress at the critical strain (e_c). Recall that up to the critical strain, the total stress is completely elastic as there is no rolling/sliding so that the applied stress is resisted entirely by elastic deformation of the structure. The compressive yield stress, P_Y , is obtained by substituting $\theta_r = \pi/2$ and $e_o = e_c$ in the expression for the normal stress in the ‘3’ direction (Eqn 17),

$$\sigma_{33} = \frac{6}{\pi} \frac{e_c z_c \alpha}{D} \phi^{\left(\frac{d-d_f+2(d_1-1)}{d-d_f}\right)} \left[\frac{k_{n,c}}{5} + \frac{2k_{t,c}}{15} \phi^{\frac{2}{d-d_f}} \right], \quad (21)$$

The simulations show that dependence of the load-bearing fraction, α , on the volume fraction can be represented by a power-law relation, $\alpha \approx 3.3\phi^{4/3}$.

In order to close the problem, the average coordination number needs to be related to the volume fraction. The former should be a monotonically increasing function of ϕ though the exact relation

would require the knowledge of the structure evolution. The z versus ϕ relation are taken from the simulation results and it is seen that average co-ordination number is invariant with volume fraction. Substituting a constant value of z and the corresponding expression for α in Equation (21) in terms of ϕ gives an explicit expression between the yield stress and the volume fraction. Note that the above expression is different from that obtained for two-dimensional colloidal gels[20].

Calculation of inter-particle force for Figure 3 of main text

(a) Silica dispersion[21]

On page 4704 of manuscript [21], bond breaking energy is mentioned as $U_d = 20 \times 10^{-21} J$ and corresponding maximum stretching in bond, $(l_d - l_0) = 0.1$ nm. Taking $U_d = F_0(l_d - l_0)$ gives, $F_0 = 0.2$ nN.

(b) Alumina dispersion [22]

On page 3312, Fig 8 of manuscript [22], the interparticle potential, U is given as $54k_B T$ while the particle radius is, $R = 0.2 \mu m$. For two spheres of identical size, the inter-particle energy due to van der Waals force is given as $U = AR/12r$, where A, r are respectively, the Hamakar constant and separation distance between particle surfaces. Assuming the Hamakar constant, $A = 10^{-20} J$, we get $r = 7.7 \times 10^{-10} m$. The van der Waals force is given as, $F_0 = AR/12r^2 = 0.28$ nN.

(c) Polystyrene dispersion [23]

The inter-particle energy is not given in Buscall [23]. The particle radius, R is $0.25 \mu m$. We assume a separation distance, $r = 0.1$ nm and $A = 10^{-20} J$, which gives $F_0 = 20.8$ nN for the van der Waals force.

[1] S. Plimpton, J. Comput. Phys., **117**, 1 (1995).

[2] C. Kloss, C. Goniva, A. Hager, S. Amberger, and S. Pirker, Prog. Comput. Fluid. Dy., **12**, 140 (2012).

[3] G. Brambilla, S. Buzzaccaro, R. Piazza, L. Berthier, and L. Cipelletti, Phys. Rev. Lett., **106**, 118302 (2011).

[4] F. Gilabert, J.-N. Roux, and A. Castellanos, Phys. Rev. E, **78**, 031305 (2008).

- [5] P. Cundall and O. Strack, *Geotechnique*, **29**, 47 (1979).
- [6] E. Furst and J. Pantina, *Phys. Rev. E*, **75**, 050402 (2007).
- [7] J. Pantina and E. Furst, *Langmuir*, **24**, 1141 (2008).
- [8] S. Roy and M. S. Tirumkudulu, *J. Rheol.*, **60**, 559 (2016).
- [9] A. Doménech, T. Domenech, and J. Cebrián, *Am. J. Phys.*, **55**, 231 (1987).
- [10] R. Seto, R. Botet, M. Meireles, G. Auernhammer, and B. Cabane, *J. Rheol.*, **57**, 1347 (2013).
- [11] W.-H. Shih, W. Y. Shih, S.-I. Kim, J. Liu, and I. A. Aksay, *Phys. Rev. A*, **42**, 4772 (1990).
- [12] R. Buscall, P. D. Mills, J. Goodwin, and D. Lawson, *Phys. Rev. E*, **53**, 3702 (1996).
- [13] K. Masschaele, J. Fransaeer, and J. Vermant, *J. Rheol.*, **53**, 1437 (2009).
- [14] F. Beer, E. R. Johnston Jr, D. Mazurek, P. Cornwell, E. Eisenberg, and S. Sanghi, *Vector mechanics for engineers*, Vol. 1 (Tata McGraw-Hill Education, 1962).
- [15] R. Buscall, P. D. Mills, J. Goodwin, and D. Lawson, *J. Chem. Soc., Faraday Trans. 1 F*, **84**, 4249 (1988).
- [16] F. Radjai, D. Wolf, M. Jean, and J. Moreau, *Phys. Rev. Lett.*, **80**, 61 (1998).
- [17] Y. Kantor and I. Webman, *Phys. Rev. Lett.*, **52**, 1891 (1984).
- [18] A. Potanin and W. Russel, *Phys. Rev. E*, **53**, 3702 (1996).
- [19] T. Nakayama, K. Yakubo, and R. Orbach, *Rev. Mod. Phys.*, **66**, 381 (1994).
- [20] S. Roy and M. S. Tirumkudulu, *J. Rheol.*, **60**, 575 (2016).
- [21] C. Parneix, J. Persello, R. Schweins, and B. Cabane, *Langmuir*, **25**, 4692 (2009).
- [22] L. Bergström, C. Schilling, and I. Aksay, *J. Am. Ceram. Soc.*, **75**, 3305 (1992).
- [23] R. Buscall, *Colloids and surfaces*, **43**, 33 (1990).